

Fast pyrolysis of agricultural residues: Reaction mechanisms and effects of feedstock properties and microwave operating conditions on the yield and product composition

Ana Karen Silos-Llamas^a, Hanifrahmawan Sudibyo^b, Virginia Hernández-Montoya^a, Will Meredith^c, Gabriela Durán-Jiménez^{c,*}

^a TecNM/Instituto Tecnológico de Aguascalientes, Av. Adolfo López Mateos No. 1801 Ote, C.P. 20256 Aguascalientes, Mexico

^b Chemical Engineering Department, Universitas Gadjah Mada, Yogyakarta 55281, Indonesia

^c Faculty of Engineering, University of Nottingham, Nottingham Park, Nottingham NG7 2RD, United Kingdom

ARTICLE INFO

Keywords:

Fast pyrolysis
Agricultural residue
Reaction mechanism
Dielectric properties
Biofuel

ABSTRACT

Fundamental understanding of the pyrolysis process plays an indispensable role in valorization of wastes and the development of novel sustainable technologies. This study introduces a novel approach by investigating the reaction mechanisms involve in Microwave-Assisted Fast Pyrolysis (MAFP) to unveil the thermal decomposition of agricultural residues: pecan nutshell (NS), sugarcane bagasse (SB), and orange seed (OS) biomasses. The holistic understanding of the pyrolysis process for these biomasses was analyzed based on the final chemical compositions and yields of bio-oil, biochar and biogas and correlated to the microwave processing conditions and feedstock's chemical composition. The findings revealed that the bio-oil is enhanced at moderated microwave energy (<5 GJ/t) as result of endothermic reactions such as heterolytic fragmentation, Maccoll elimination, Friedel-Craft acylation, Piancatelli rearrangement and methoxylation. The maximum yield of bio-oil for protein-rich biomass was due to selective heating (Paal-Knorr pyrrole synthesis, Baeyer-Villiger oxidation, Maillard reaction, and ring conversion of γ -butyrolactone). The formation of biochar and biogas is attributed to the re-polymerization of aromatic aldehydes, hydrocarbons, amines, and ethers, as well as dehydroxymethylation and dealkylation processes. This study provides a comprehensive understanding of the reaction mechanisms for several wastes using microwave pyrolysis, to establish the bases for effective valorization and agricultural waste management.

1. Introduction

Agri-industry generated substantial amount of residues every year as a consequence of massive production of various nutritious food to match the increasing global food demand. For instance, ~2 billion metric tons of sugarcane bagasse [1], 1.5 million metric tons of pecan nutshell [2,3], and ~20 million metric tons of orange seed [4] are produced annually by the sugar, nut, and juice industries in the world. Traditional management of these residues include direct combustion and dumping at landfill site. These methods unfortunately release carbon to the atmosphere and nutrients into water basins, potentially causing several environmental threats including global warming, eutrophication and acidification of water bodies, and pathogen spread [5–7]. Development of innovative technologies to sustainably recover resources contained in

agricultural residues is pivotal, not only to prevent the environmental pollutions, but also to acquire economic and environmental benefits from valorizing biomass into valuable products.

Pyrolysis is a promising thermochemical process operating at 300–700 °C and 5–20 bar in the absence of oxygen, capable of promoting the conversion of organic and inorganic macromolecules of biomass into several derivative compounds distributed into three product phases, i.e., bio-oil, solid biochar, and biogas [8]. The bio-oil is rich in carbon and contains a significant concentration of high-valued fine chemicals that can be separated and recovered through fractionation in refineries [9]. A mixture of low-concentration carbon-dense compounds in the bio-oil can also be employed as energy source for generating renewable heat and electricity [10,11]. The solid biochar contained a high content of nutrient and a considerable amount of

* Corresponding author.

E-mail address: Gabriela.Duranjimenez1@nottingham.ac.uk (G. Durán-Jiménez).

<https://doi.org/10.1016/j.jaap.2023.106217>

Received 29 August 2023; Received in revised form 26 September 2023; Accepted 9 October 2023

Available online 11 October 2023

0165-2370/© 2023 The Author(s). Published by Elsevier B.V. This is an open access article under the CC BY license (<http://creativecommons.org/licenses/by/4.0/>).

carbon useful for soil amendment or soil fertilizer [12]. The biogas contained a high concentration of syngas and gas-phase hydrocarbon beneficial for the production of chemical building blocks [13]. The characteristics of the three product phases highlight the potential key roles of pyrolysis in valorizing the agricultural residues.

According to the heating rate, pyrolysis is classified into slow, fast, and flash pyrolysis with the time scale of respective process is in the order of hours, minutes, and seconds [14]. Slow pyrolysis is favored for the accomplishment of high yield of biochar [15], whereas the fast and flash pyrolysis are favored to produce a higher yield of bio-oil and biogas [16]. Given the much larger potential economic and environmental benefits of the utilization of fine chemicals and high energy content in bio-oil and biogas than the direct use of biochar as solid biofuel and soil amendment/fertilizer [17–19], fast and flash pyrolysis are of greater interest. Due to the extremely quick heating rate of flash pyrolysis and the requirement of material of construction of reactor that can handle high leap of temperature while keeping a very-low heat loss, only fast pyrolysis has reached the pilot and commercial scales operation with a processing capacity that ranges from 250 to 1000 ton/day [20,21]. The developed commercial fast pyrolysis equipment employs microwave systems providing a heating rate of 10–50 °C/min.

Despite successful scale-up of microwave-assisted fast pyrolysis (MAFP) to commercial scale, there are still limited information and evaluation on fundamentals of reaction mechanisms leading to the formation of products and the transformation of elemental speciation during the MAFP of feedstocks with combined macromolecules compositions at various operating conditions. Previous mechanistic studies on fast pyrolysis of biomass focused on the conversion route of pure microcrystalline cellulose, levoglucosan, and hemicellulose representing the carbohydrate fraction and phenylphenethyl ether, diphenyl ether, and ortho-methoxyphenol to represent the lignin fraction. For instance, Wang and coworkers [22] discovered three main pyrolytic transformation pathways of cellulose through experimental-validated molecular simulation approach, i.e., homogeneous cleavage, retro-aldol condensation, and dehydration yielding levoglucosan, glycolaldehyde, and 5-hydroxymethylfurfural, respectively. Later on, Osatiashiani and coworkers [23] provided more detailed insights into decomposition of levoglucosan into anhydro sugars, furan, and furfural under no catalytic condition. Moreover, they found that the application of HZSM-5 catalyst promote further derivation of furanic compounds into monoaromatics and polyaromatics in bio-oil. Carrier et al. [24] reported that hemicellulose fraction in the biomass is the main contributor of small oxygenates and short-chain aliphatic acids in the bio-oil.

Meanwhile, Custodis et al. [25] identified two main decomposition routes for decomposition of diphenyl ether and *o*-methoxyphenol: (1) the homolytic fission of the weakest bond-forming radicals and (2) the radical initiation yielding different radicals that can rearrange and recombine. They also emphasized that the degree of substitution is critical in the stabilization of intermediate radicals and the degree of recombination prefers the phenoxy radicals compared to hydroxy-phenoxy radicals. Using the same pure compounds coupled with HZSM-5 catalysts, Luo and coworkers [26] reported that the main decomposition pathways of lignin are cyclization reactions yielding aromatic hydrocarbons, while direct demethylation, demethoxylation and dehydration reactions are considered the secondary pathways converting phenolic lignin monomers into aromatic hydrocarbons.

Although these earlier studies present useful mechanistic information, the actual reaction pathways are potentially different when the primary macromolecules of biomass including carbohydrate, lignin, protein (N-source), and lipid coexist in real feedstocks, e.g., agricultural residues. Therefore, our approach focused on three main objectives: (1) processing three agricultural residues with different macromolecule profiles (i.e., pecan nutshell (NS), sugarcane bagasse (SB), and orange seed (OS)) at different microwave power intensity (300–400 W) and different processing times (3–5 min), (2) characterizing the effects of feedstocks' dielectric properties and operating conditions on the yield

and chemical composition of MAFP products derived from the three investigated biomass, and (3) evaluating the most significant reaction mechanisms underlying the observed trend of products yields.

Pecan nutshell was selected as it contains a mixture of lignin, hemicellulose, and extractives including flavonoids and tannins [27]. Sugarcane bagasse was picked since it is mostly constituted by lignin and cellulose [28]. Orange seed was chosen because of balanced combination of carbohydrate, fiber, protein, and fat [29]. The dielectric properties of the three feedstocks including the dielectric constant and loss were measured to explain the ability of biomass to absorb the microwave energy and to convert the absorbed microwave energy into heat, respectively. The measured dielectric properties and the operating conditions were correlated with the measured yield and chemical composition of products. The observed correlations was explained from a mechanistic point of view by making use of the reaction pathways developed by implementing a heuristic graphical approach based on the chromatographic composition of bio-oil and biogas. Results in this study inform a comprehensive list of reaction mechanisms and corresponding operating conditions leading to the formation of specific chemicals in the pyrolysis products.

2. Materials & methods

2.1. Pyrolysis feedstocks




The investigated agricultural residues in this study were pecan nutshells (NS) (*Carya illinoensis*), sugarcane bagasse (SB) and orange seed (OS) (*Citrus sinensis*) collected from different agricultural industries in Aguascalientes State (Mexico). The three feedstocks were initially milled and sieved to achieve a relatively uniform particle size of ≤ 1 mm. Afterwards, they were washed with deionized water until constant pH and was finally oven-dried (Companion OF 01E) at 70 °C for 24 h.

In order to increase the microwave susceptibility in NS, SB and OS, the dried biomass powders were pelletized using an Atlas hydraulic press (Specac Atlas Automatic 25 Ton) in a cylindrical moulding with 32 mm in diameter and 10 mm in thickness. Details of pelletization conditions are given in Table 1.

2.2. Physicochemical characterizations of biomass

Thermogravimetric experiments were performed in triplicate to characterize the content of volatile matter, fixed carbon, and ash following the method previously described by Donahue and coworkers [30]. Briefly, the sample was placed in TGA Q500 TA Instrument and heated to 900 °C under a N₂ atmosphere (100 mL/min, 1 bar), and then held at 900 °C for 15 min. The atmosphere then was switched to air and held for a further 15 min. The outcomes of this analysis also include the generation of thermogravimetric (TG) and differential thermogravimetric (DTG) curves useful to extract the thermal properties of

Table 1
Conditions of pelletization for the investigated agricultural residues.

Biomass	Mass (g)	Pressure (Ton)	Time (min)	3D Visual	Density kg/m ³
Pecan nutshell (NS)	10	8	30		113
Sugarcane bagasse (SB)	7	8	30		79
Orange seeds (OS)	15	5	5		170

feedstocks at higher temperatures. The triplicated ultimate analysis (LECO CHN 628) following the ASTM D5373–21 protocol was carried out to measure the content of carbon, hydrogen, nitrogen, and oxygen. The chemical functionalities of the feedstocks were identified using Fourier-Transform Infrared (FTIR) spectroscopy (ThermoScientific Nicolet iS10) with attenuated total reflectance (ATR) accessory. The FTIR spectra were recorded from 4000 to 400 cm^{-1} with a resolution of 4 cm^{-1} and averaged over 3 replicate scans.

The dielectric constant (ϵ') and loss factor (ϵ'') were determined using the cavity perturbation technique [31] at 2.45 GHz from room temperature to 650 °C. Certain amount of the biomass was packed in a quartz tube with an internal diameter of 3 mm. The sample was heated up in a Carbolite furnace and once the desired temperature was reached, the sample was returned to the cavity position (i.e., by means of an automatic motor) where the measurement was recorded. A vector network analyser measured the change in frequency and the resulting value of the Q factor of the empty and loaded tube. The response of the feedstock to the electromagnetic field was mathematically defined by their dielectric properties represented by the complex permittivity described in Eq. 1. The dielectric constant and loss factor were calculated using the Maxwell's equations in Eq. 2 and Eq. 3.

$$\epsilon = \epsilon_0 \epsilon^* = \epsilon_0 (\epsilon' - j) \quad (1)$$

$$\epsilon' = 1 + 2(j_1^2(X_{l,m})) \left(\frac{V_o}{V_s} \right) \left(\frac{f_o - f_1}{f_o} \right) \quad (2)$$

$$\epsilon'' = (j_1^2(X_{l,m})) \left(\frac{V_o}{V_s} \right) \left(\frac{1}{Q_1} - \frac{1}{Q_o} \right) \quad (3)$$

The ϵ_0 is the permittivity of free space ($8.854 \cdot 10^{-12} \text{ F}\cdot\text{m}^{-1}$), ϵ^* is a complex permittivity, and j is an imaginary magnitude ($j^2 = -1$). The j_1 is the first-order coefficient of the Bessel function, $X_{l,m}$ is the n^{th} and the first order root of Bessel function, V_o is the cavity volume (mm^3), V_s is the sample volume (mm^3), f_o is the frequency resonant void cavity (GHz), and f_1 is the resonant cavity loaded with sample (GHz). The Q_o is the Q factor of the empty cavity and Q_1 is the Q factor of the sample-loaded cavity.

2.3. Microwave-assisted fast pyrolysis experiment

The microwave-assisted fast pyrolysis (MAFP) experiment was conducted in a microwave system as illustrated in Fig. 1. The system comprising a 2-kW single-mode Sairem® (2.45 GHz) applicator integrated with an automatic homer tuner (S-TEAM STHD v1.5), and a single mode applicator where the quartz reactor was placed [32]. In each experiment, the biomass pellet was placed in a quartz tube connected to a condenser and flask in an ice bath at 4 °C where the bio-oil and biogas was later collected. In order to provide an oxygen-free environment, a nitrogen flow of 2 L/min was fed into the microwave system. Noteworthy was that it was unfeasible to accurately record the sample temperature as the use of thermocouples affected the homogeneity of microwave power distribution in the cavity. Thus, microwave power intensity and processing time were the investigated operating parameters, as shown in Table 2. The calculated specific energy represented the combined effect of the microwave power intensity and processing time with the various dielectric feedstocks. This parameter was useful in understanding how dielectric properties affected the absorbed energy, measured yield and chemical composition of products.

The homer tuner measured profiles of the power input, the reflected power and the power absorbed by the solid feedstock during the

Table 2

Details of operating conditions and absorbed energy for microwave-assisted fast pyrolysis experiments of pecan nutshell (NS), sugarcane bagasse (SB), and orange seed (OS).

Sample Code	Power (W)	Time (min)	Specific Energy (kJ/g)
B-NS-300-4	300	4	4.81
B-NS-300-5	300	5	6.12
B-NS-400-3	400	3	5.22
B-SB-300-4	300	4	4.49
B-SB-300-5	300	5	9.37
B-SB-400-3	400	3	6.07
B-OS-300-4	300	4	1.86
B-OS-300-5	300	5	4.06
B-OS-400-3	400	3	3.42

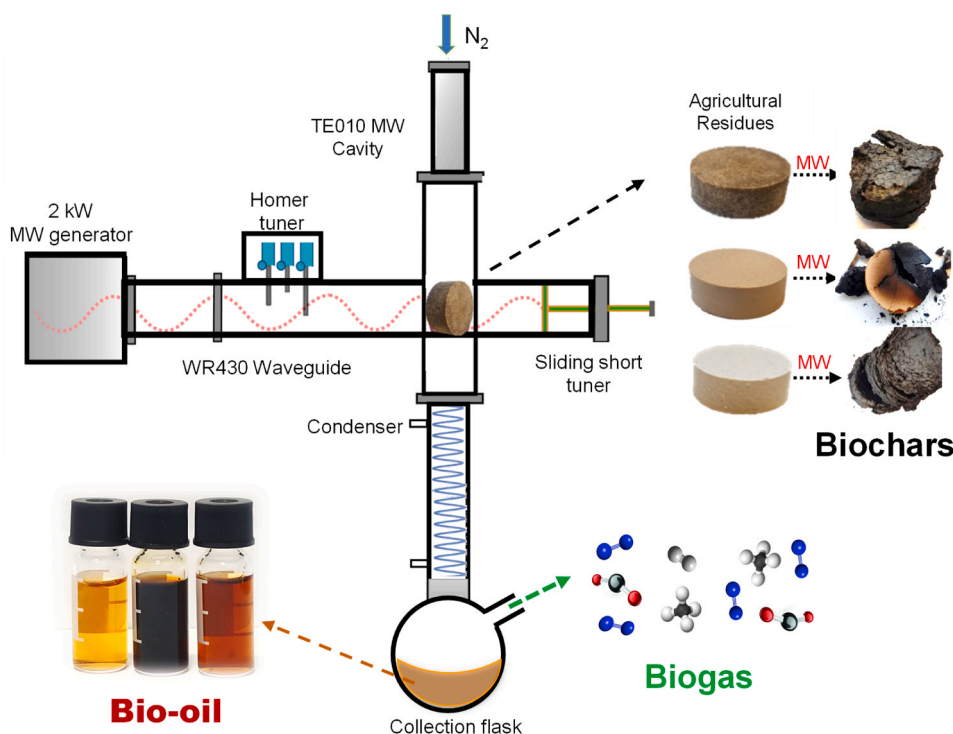


Fig. 1. Schematic representation of MAFP system used in this study.

experiment. The specific absorbed energy (E , kJ/kg) by certain mass of feedstock (m , g) was determined by numerical integration (see Eq. 4) of the absorbed power (P_a , W) measured and recorded over time (t , s) by the homer [33]. Representative incident and absorbed powers profiles during MAFP experiment was shown in Fig. S1 in the Supporting Information document.

$$E = \frac{1}{m} \int_{t=0}^{t=t} P_a \cdot dt \quad (4)$$

Once the MAFP experiment finished, the condensed bio-oil was recovered, the solid biochar was collected, and the non-condensable gasses were stored in a 500 mL Tedlar gas bag for compositional analysis. The mass yield of each product was calculated by dividing the measured weight of each product phase with the dry weight of feedstock. Fig. 1 illustrates the MAFP system used in this study.

2.4. Compositional analysis of bio-oil and biogas

The chromatographic composition of the biogas was measured using Clarus 580 Gas Chromatograph (GC) system. The hydrocarbons and non-hydrocarbons components were detected using FID and TCD detectors. In general, 5 mL of sample the sample was injected at 250 °C using helium as gas carrier and a 30 m x 0.32 mm x 10 µm fused silica column for the separation. The chromatographic composition of the bio-oil was semi-quantitatively characterized by a Varian CP-3800 GC incorporated to a Varian 1200 MS (70 eV, EI mode, full SCAN m/z 40–450). The column used was DB-1701, low to middle polarity with stationary phase thickness. The oven temperature profile was 50 °C held for 2 min, and 5 °C/min to 280 °C, held for 16 min. Helium was used as the carrier gas at a constant flowrate of 1.2 mL/min. The semi-quantitative composition of detected compounds in the bio-oil was derived from the relative peak area percentage, assuming an equal response factor for each detected compound. The identification of each individual compounds was done by comparing the obtained GC-MS spectra with the National Institute of Standards Technology (NIST) database [32,34].

2.5. Reaction pathways construction

The conversion pathways of each feedstock were constructed by using the MØD cheminformatic software [35]. The starting compounds was based on the primary macromolecules described in the literature and was approached by a group of simple polymeric compounds, e.g., cellobiose [36], phenylalanine [37], 1-(3,4-dimethoxyphenyl)-2-(4-hydroxy-2-methoxyphenoxy)propane-1,3-diol [38], and triolein [39] to represent polysaccharides, protein, lignin, and lipid, respectively. The propensity of potential chemical reactions (i.e., based on theoretical chemistry in the literature) from these starting compounds toward the detected compounds in the bio-oil and biogas were inputted into the software. The MØD cheminformatic software subsequently generated hypothetical reaction pathways, including hypothetical intermediates that may or may not be detected in bio-oil and biogas, based on the chemical graph transformation rules whose parameter settings followed the Double-Pushout approach specified in the literature [40, 41]. Ultimately, each hypothetical reaction path was evaluated for the change of Gibbs free energy (ΔG , estimated using eEquilibrator [42] in order screen the most thermodynamically-feasible pathways, i.e., $\Delta G < 0$.

3. Results & discussion

3.1. Physicochemical characteristics of biomass

3.1.1. Elemental content and proximate composition

Table 3 shows the proximate and elemental compositions of the

Table 3

Proximate and elemental compositions of pecan nutshell (NS), sugarcane bagasse (SB), and orange seed (OS) employed as feedstocks in this study.

Parameters	Feedstocks			
	Pecan Nutshells (NS)	Sugarcane Bagasse (SB)	Orange Seed (OS)	
Elemental Content	C (wt%)	48.9 ± 0.3	43.6 ± 0.1	55.5 ± 0.3
	H (wt%)	6.0 ± 0.0	6.2 ± 0.4	8.5 ± 0.0
	N (wt%)	0.2 ± 0.0	0.9 ± 0.0	2.1 ± 0.1
	*O (wt%)	44.8 ± 0.4	49.3 ± 0.5	33.9 ± 0.3
Proximate Composition	Moisture (%)	6.2 ± 0.3	5.8 ± 0.3	5.6 ± 0.28
	Volatile matter (%)	77.2 ± 3.9	82.5 ± 4.1	81.2 ± 4.1
	Fixed carbon (%)	14.8 ± 0.7	7.8 ± 0.4	10.6 ± 0.5
	Ash (%)	1.8 ± 0.1	3.8 ± 0.2	2.5 ± 0.1
	Estimated higher heating value (HHV, MJ/kg)	17.8 ± 0.9	15.8 ± 0.8	16.9 ± 0.8

* Calculated by difference.

investigated feedstocks for MAFP experiments. The obtained values for the composition of moisture, volatile matter, fixed carbon, and ash and the content of carbon, hydrogen, nitrogen, and oxygen were consistent with the reported values in the literature [43–45]. It is evident the carbon content and fixed carbon are higher in NS and OS than the values found for SB feedstock. Interestingly, SB showed higher content of ash and volatiles (3.8% and 82.5%, respectively) than NS and OS. The chemical composition of feedstocks (volatile matter, fixed carbon, ash content, and composition of carbohydrate and protein (i.e., indicated by the nitrogen content)) is fundamental to understand the formation and distribution of bio-oil, biochar, and biogas. This information is fully discussed in Section 3.2.

The TG and DTG curves of the three feedstocks are shown in Fig. 2. In general, the maximum weight loss was attained at approximately 335, 356 and 388 °C for SB, NS and OS, respectively. The mass loss due to the thermal transformation of the three feedstocks occurred in three stages from room temperature to 800 °C. The first stage, from room temperature to around 120 °C, was associated with the weight loss caused by the initial evaporation of moisture. The second stage, which showed a mass loss greater than 75% in the range of 200–500 °C, as attributed to the decomposition of less-stable bio-polymers including cellulose and hemicellulose [46,47]. The third stage represented the decomposition of more complex non-digested fibres including lignin in a wide range of temperatures of 200–600 °C [48,49].

3.1.2. Functional groups

Fig. 3 shows the FTIR spectra of the three feedstocks. Most of the identified peaks in the FTIR spectra of the three feedstocks were highly similar. The pronounced peak at 3346 cm^{-1} was attributed to the O-H stretching of phenols and aldehydes [50,51]. A doublet was observed at 2932 and 2856 cm^{-1} , associated with the symmetric and asymmetric stretching of the C-H bond of alkanes, alkenes, and aldehydes, respectively [52]. The peak at 1770 cm^{-1} was related to the C=O stretching of carboxylic acids, esters, and ethers [53]. The peak at 1645 cm^{-1} was characteristic of C=C stretching of aromatic structures [54]. The functional groups with broad peak at 1031 cm^{-1} were the C–O stretching of alcohols and polysaccharides [55].

3.1.3. Dielectric profiles

The dielectric constant (ϵ') and the dielectric loss factor (ϵ'') of the

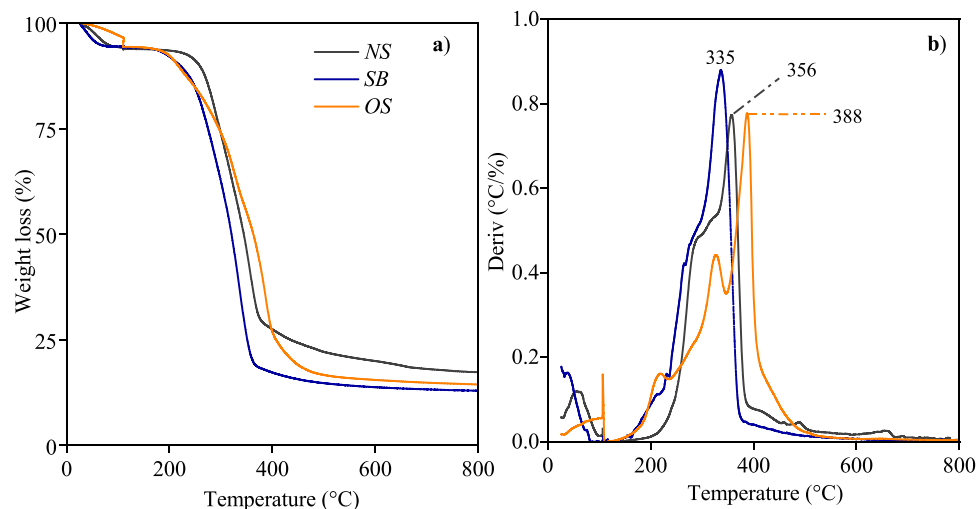


Fig. 2. Thermal properties of pecan nutshells (NS) sugarcane bagasse (SB), and orange seed (OS).

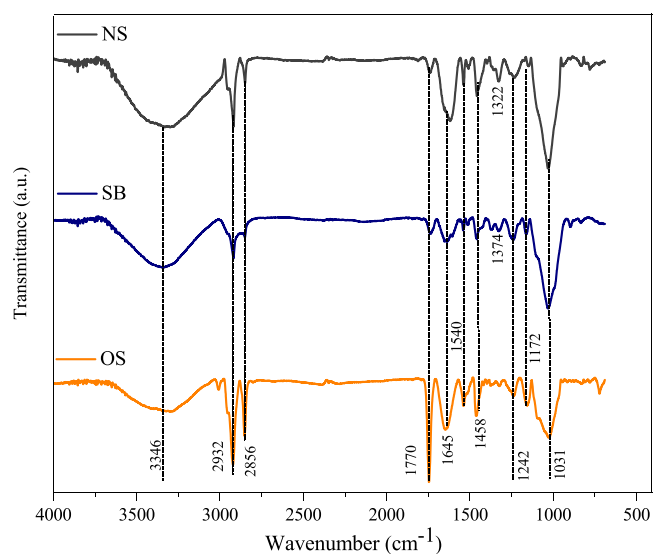


Fig. 3. FTIR spectra of pecan nutshell (NS), sugarcane bagasse (SB), and orange seed (OS).

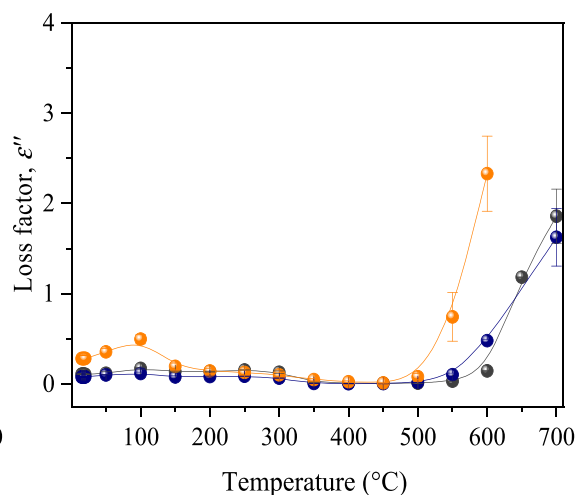
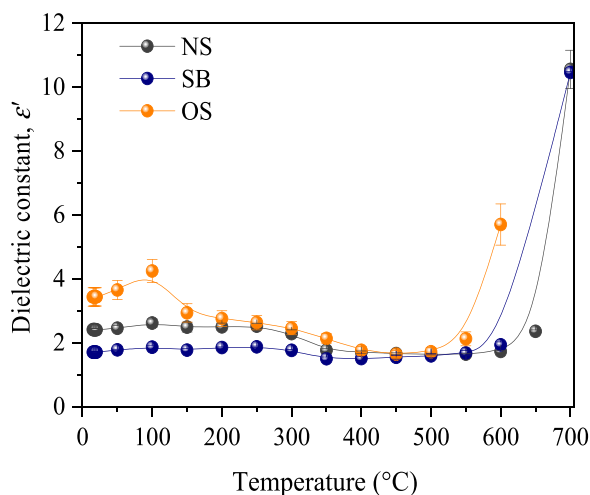


Fig. 4. The dielectric constant (ϵ') and dielectric loss factor (ϵ'') of pecan nutshell (NS), sugarcane bagasse (SB), and orange seed (OS) measured at 2450 MHz from 25° to 650°C.

three biomass feedstocks were determined by the cavity perturbation technique from 25° to 650°C. Fig. 4 reveals three regions representing a significant change of dielectric properties at higher temperatures. The first change was observed from room temperature to 100 °C due to the evaporation of water, which is a strong microwave absorber. After the removal of free-bonded water, the dielectric properties of biomass decreased in the region between 100 and 500 °C. The polar components in cellulose and hemicellulose were polarised from 300° to 400°C, promoting the pyrolysis and breaking of less thermo-stable molecular chains leading to molecular rearrangement of the biomass. This decrease was consistent with the maximum mass loss observed in the DTG and TG analyses (see Fig. 2) and with the decomposition profile of cellulose [32, 56]. According to the literature [53,57], when biomass is subjected to higher temperatures (> 500 °C), the structure become essentially carbonaceous, known to be a high microwave absorbent material due to the Maxwell–Wagner effect. This phenomenon causes a very high displacement of π -electrons on carbonized structures, resulting on an exponential increase in the dielectric constant and loss factor [58].

3.2. Product yield distribution

Fig. 5 shows that the obtained mass yield of bio-oil, biochar, and biogas ranged from 5% to 22%, from 15% to 47%, and from 41% to 71%,

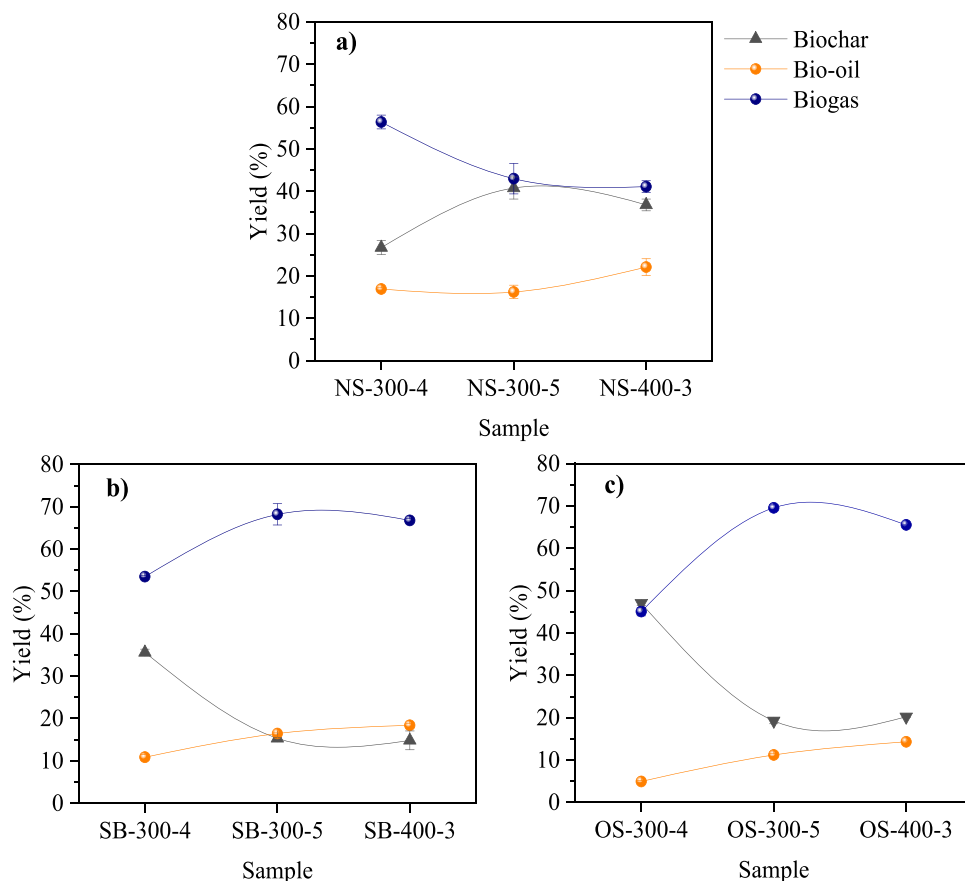


Fig. 5. Mass yield distribution of bio-oil, biochar, and biogas produced from microwave-assisted pyrolysis of NS (a), SB (b) and OS (c) at 300–400 W and processing time of 3–5 min.

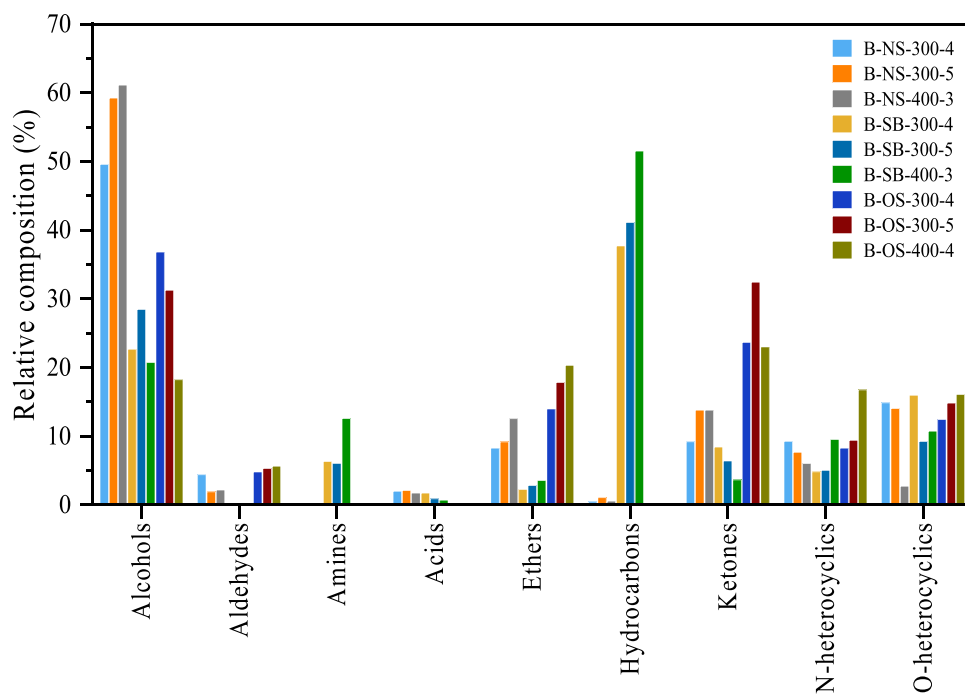


Fig. 6. Distribution of chemical groups in the bio-oil produced from microwave-assisted pyrolysis of pecan nutshell (NS), sugarcane bagasse (SB), and orange seed (OS) at 300–400 W and processing time of 3–5 min.

respectively. In general, increasing the microwave power input and prolonging the processing time improved the yield of bio-oil. The three-minute processing time and 400-W microwave power input, which was equivalent to specific energies of 4.22, 6.07 and 3.42 kJ/g for NS, SB, and OS, respectively, produced the highest bio-oil yield, i.e., 22%, 18%, and 14% for NS, SB, and OS, respectively.

Fig. 6 shows that the enhanced bio-oil formation from NS, SB, and OS at higher microwave power input and extended processing time was associated with the increased formation of (1), phenols, ethers, and ketones; (2) phenols, hydrocarbons, amines, N-heterocyclics, and ethers and (3) aldehydes, ethers, N-heterocyclics, O-heterocyclics, and ketones, respectively. Detailed explanations on their formation mechanisms are given in subsection 3.3.

A higher biochar yield was observed from the MAFF of NS at higher microwave power input and longer processing time. As the bio-oil and biochar yields from the MAFF of NS showed an increasing trend with microwave power input and processing time, it was expected that the yield of biogas comprising carbon dioxide, methane, propene, and hydrogen (see Table S1) showed a decreasing trend.

Meanwhile, the biogas yield from the MAFF of SB and OS showed an increasing trend with microwave power input and processing time. Combined with the decreasing trend of biochar yield from the MAFF of SB and OS at higher microwave power input and longer processing time, this result provided two interpretations. First, this result may suggest that the biogas formation was due to the decomposition of organics contained in the SB and OS or the biochar. Second, this result may indicate that the solid organics in the two feedstocks or biochar first underwent transformation into chemical species with smaller molecular weight in the bio-oil, before experiencing partial decomposition into gaseous compounds contributing to the improvement of the biogas yield [59]. The acquired composition of biogas was generally similar to that derived from NS (i.e., methane, carbon dioxide, propene, and hydrogen), with additional presence of carbon monoxide and acetylene in the biogas from OS, as shown in Table S1.

When comparing the outcomes of MAFF of different feedstocks at similar operating conditions, the bio-oil yield decreased in the following order, i.e., NS > SB > OS. This result was contradictory with the order of volatile matter (i.e., main contributor of the bio-oil [60,61]) content that decreased in the following order, i.e., SB > OS > NS (see Table 3). The presence of protein as a macromolecule in the NS was predicted to be the cause of this observation. The protein may lead to the occurrence of Maillard reaction providing synergistic effects toward the bio-oil yield [62–64]. The synergistic effect was defined as the higher value of measured bio-oil yield from a mixture of compounds than the mass-averaged bio-oil of individual pure compounds. The course of Maillard reaction in the MAFF of NS was discussed in subsection 3.3.1.

At similar sets of microwave power input and processing time (i.e., 300 W and 5 min and 400 W and 3 min), the biochar yield decreased in the following order, i.e., NS > OS > SB. This order agreed with the total content of fixed carbon and ash in the investigated feedstocks. Fixed carbon is the solid combustible residue remaining after biomass feedstock is heated and the volatile matter is transformed into bio-oil and biogas [59]. Meanwhile, ash represents the inorganic matrix of biomass, and these inorganics were expected to be distributed only into the solid biochar phase due to their physicochemical characteristics [65].

At lower microwave power input (300 W) and shorter processing time (4 min), the biochar yield increased in the following order, i.e., NS < SB < OS. The higher biochar yield of SB and OS than NS were due to the repolymerization of chemical species in bio-oil, as evidenced by the reduced bio-oil formation in the following order, i.e., NS > SB > OS. The higher vulnerability of compounds in bio-oil from SB and OS toward repolymerization into hydrochar rather than partial decomposition into biogas was also confirmed by the increased production of biogas in the following order at the same reaction conditions, i.e., OS < SB < NS. However, the biogas yield showed a reverse trend (i.e., NS < SB < OS) at different sets of microwave power input and processing time, i.e., 300 W

– 5 min and 400 W – 3 min. This result was attributed to the increased decomposition of derivatives of highly-abundant polysaccharides in SB and OS into biogas [66].

3.3. Mechanistic explanations

Subsections 3.3.1–3.3.4 provide comprehensive mechanistic explanations on the effects of microwave power input and processing time toward the observed yield of products and the formation of each chemical species produced from each feedstock. The explanations were based on the proposed reaction pathways for the MAFF of NS, SB, and OS shown in Fig. 7. This figure shows each pathway with the labels H#, L#, and P# where H, L, and P represent the initials of holocellulose, lignin, and protein, respectively, and # indicates the reaction pathway number. These reaction pathways were derived from the heuristic graphical approach validated by chemical composition of the bio-oil and biogas, as shown in Table S1. Given the different composition of primary organic macromolecules of NS (e.g., lignin, holocellulose, amino acids, and extractives including flavonoids and tannins integrated to lignin structure [27]), SB (e.g., lignin, holocellulose, and protein [28]), and OS (e.g., fat, carbohydrate, fiber, and protein [29]), the diverse compositions of the bio-oil were expected. Likewise, relatively uniform biogas compositions were expected because the partial decompositions of bio-oil constituents into gaseous compounds mostly involved the dealkylation, decarboxylation, decarbonylation, and dehydrogenation.

3.3.1. Pecan nutshell (NS)

The pyrolytic conversion of pecan nutshell produced bio-oil that was mostly composed of phenols (e.g., 2-methoxyphenol, 2-methoxy-6-methylphenol, 4-ethyl-2-methoxyphenol, *o*-cresol, vanillin, 2-methoxy-4-propylphenol, 2,6-dimethoxy-4-(2-propenyl)-phenol, and 2,6-dimethoxyphenol), ketones (e.g., 1-(2-hydroxymethylphenyl)ethanone, 1-(4-hydroxy-3-methoxyphenyl)propan-1-one, 2',6'-dimethoxyacetophenone, and 1-(4-hydroxy-2-methoxyphenyl)ethanone), and ethers, e.g., 1,2,4-trimethoxybenzene and 1,2,4-trimethoxy-5-methylbenzene. The formation of alkoxyphenols and dialkoxyphenols implied that lignin in NS was constituted by the syringyl (S) and guaiacyl (G) monomeric units through the interconnected ester bonds of monolignols sinapyl and coniferyl alcohols [67]. Moreover, the formation of alkoxyphenols and dialkoxyphenols showed the occurrence of the concerted (heterolytic) retro-ene fragmentation and Maccoll elimination mechanisms (L1, L5, L6, L12, L14, and L24) cleaving the β -ether bonds of S-lignin and G-lignin [68]. Since these mechanisms were endothermic [69], it was anticipated that higher reaction severity (i.e., higher microwave power input and longer processing time) enhanced their production in bio-oil.

Both alkoxyphenols and dialkoxyphenols subsequently underwent various conversion reactions leading to the formation of additional bio-oil components and biogas constituents. For instance, 2-methoxyphenol underwent demethoxylation and ortho-formylation (the Reimer–Tiemann reaction) producing salicylaldehyde (L16). The dehydration (L22) and reduction (L17) of salicylaldehyde yielded *o*-cresol and salicyl alcohol. The latter was further derived into 1-(2-hydroxymethylphenyl)ethanone and benzene via the Friedel–Craft acylation and a series of decarbonylation (L18) and dehydration (L19), respectively. Although the Friedel–Craft acylation was exothermic [70], the formation of 1-(2-hydroxymethylphenyl)ethanone was enhanced at more severe operating conditions due to the abundant supply of salicylaldehyde from the endothermic Reimer–Tiemann reaction [71]. The endothermicity of this reaction also led to improved generation of *o*-cresol.

Nonetheless, the effects of reaction severity on benzene formation was unclear as it was undetected in the bio-oil due to the Ullman coupling reaction (L10) with propylbenzene. The propylbenzene was obtained from the demethoxylation (L8) of 2-methoxy-4-propylphenol intermediate. The Ullman coupling reaction involved consecutive endothermic additions of propylbenzene into benzene [72], reducing

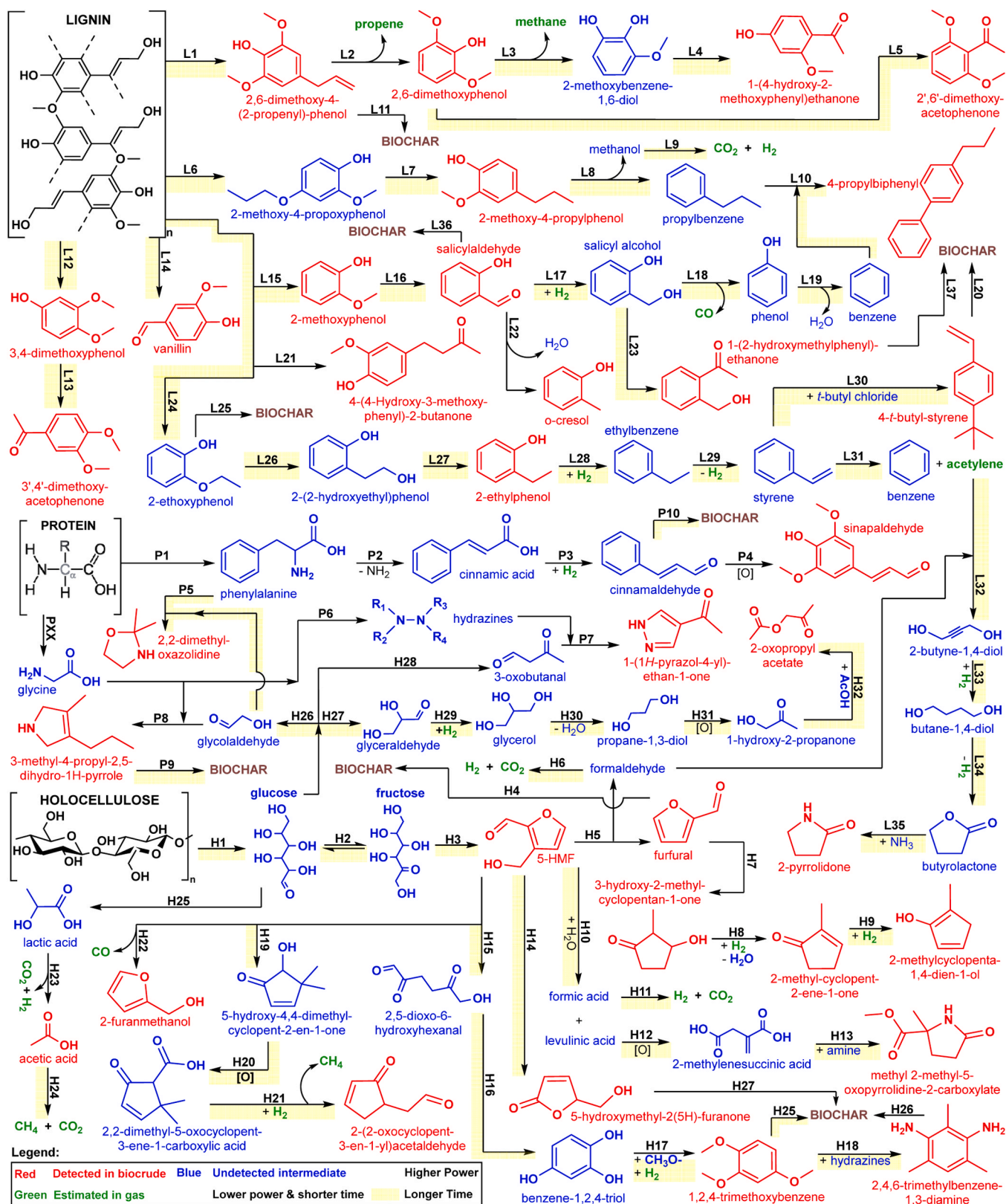


Fig. 7. Proposed reaction mechanisms for chemical formation in bio-oil and biogas from fast pyrolysis of NS, SB, and OS at microwave power input of 300–400 W and processing time of 3–5 min. Each pathway is labelled with L#, P#, and H# where L, P, and H represent lignin, protein, and holocellulose macromolecules, respectively, and # is the reaction number.

aromatic hydrocarbon (i.e., 4-propylbiphenyl) at more intensive microwave power input and prolonged processing time.

A series of endothermic dealkylation of 2,6-dimethoxy-4-(2-propenyl)-phenol provided 2,6-dimethoxyphenol (L2) and 2-methoxybenzene-1,6-diol (L3) with gaseous propene and methane as the side products, respectively. Both 2,6-dimethoxyphenol and 2-methoxybenzene-1,6-diol were prone to the Friedel-Craft acylation forming 2',6'-dimethoxy-acetophenone (L4) and 1-(4-hydroxy-2-methoxyphenyl)ethanone (L5), respectively. Similar to the 1-(2-hydroxymethylphenyl)ethanone, the increased formation of 2',6'-dimethoxy-acetophenone and 1-(4-hydroxy-2-methoxyphenyl)ethanone at more severe reaction conditions were due to the massive supply of corresponding precursors by the endothermic dealkylation of corresponding alkoxyphenols [73].

While ether structure naturally existed in lignin, the presence of ethers in the bio-oil was due to the conversion of cellulose derivatives. Cellulose underwent homolytic cleavage of the glycosidic bond to form glucose (H1), which was epimerized (H2) into fructose. Fructose was convertible into 5-(hydroxymethyl)furfural (5-HMF) via ring-opening and dehydrative cyclization (H3). The hydrolytic ring-opening and keto-enol tautomerism (H15) of HMF yielded 2,5-dioxo-6-hydroxyhexanal [74]. The 2,5-dioxo-6-hydroxyhexanal contained active α -H atoms attached to carbon number 3, 4, and 6. These active hydrogen atoms may undergo intramolecular cyclization forming 2,5-dihydroxy-1,4-benzoquinone intermediate susceptible to β -elimination and keto-enol tautomerism into 1,2,4-benzenetriol (H16). Ultimately, the replacement of hydroxyl groups of 1,2,4-benzenetriol via dehydration followed by methoxylation and subsequent methylation (H17) produced aromatic ethers, i.e., 1,2,4-trimethoxybenzene and 1,2,4-trimethoxy-5-methylbenzene, respectively. Since the whole mechanisms were endothermic [75,76], the formation of aromatic ethers increased at higher reaction severity.

In addition to phenols, ketones, and ethers, N-heterocyclics (e.g., 2,2-diethyl-3-methyl-oxazolidine) and carboxylic acids (e.g., acetic acid) were observed in the bio-oil. The 2,2-diethyl-3-methyl-oxazolidine was formed via the Maillard reaction (P5) between glycolaldehyde (i.e., derived from retro-aldol condensation of glucose, H26) and aromatic amino acids (e.g., phenylalanine and histidine) derived from pyrolytic fragmentation of protein (P1) [77]. However, the formation of 2,2-diethyl-3-methyl-oxazolidine decreased with microwave power input and prolong processing time due to the exothermic nature of Maillard reaction [78,79].

Glucose was also rearrangeable into lactic acid via the Lobry de Bruyn-Alberda van Ekenstein transformation and benzylic rearrangement (H25) [80]. The lactic acid then underwent oxidative dehydrogenation and decarboxylation (H23) into acetic acid [81]. Higher microwave power input and longer reaction time provoked partial decomposition of acetic acid into methane and carbon dioxide, primary constituents of the resulting biogas. The production of carbon dioxide, with hydrogen, was also enhanced by the endothermic dehydrogenation of formic acid (H11), methanol (L9), and formaldehyde (H6). Formic acid was acquired via rehydration of fructose-derived 5-HMF (H10), methanol was obtained as byproduct of demethoxylation of alkoxyphenols (L8), and formaldehyde was byproduct of the removal of hydroxymethyl substituent (H5) of 5-HMF into furfural [82]. Coupled with the dealkylation (L2) products of 2,6-dimethoxy-4-(2-propenyl)-phenol, the NS-derived biogas was a mixture of methane, carbon dioxide, hydrogen, and propene.

3.3.2. Sugarcane bagasse (SB)

The MAFP of SB produced bio-oil with primary constituents including phenols, hydrocarbons, amines, N-heterocyclics, and ethers. The same compounds as those detected in NS-derived bio-oil was also observed, e.g., 2,6-dimethoxyphenol, 2,6-dimethoxy-4-(2-propenyl)phenol, 5-HMF, furfural, 2',6'-dimethoxyacetophenone, acetic acid, and 1,2,4-trimethoxybenzene.

The 5-HMF, furfural, acetic acid, and 1,2,4-trimethoxybenzene were

characteristic products of cellulose derivatives, whose formation mechanisms have been explained in subsection 3.3.2. Nevertheless, the presence of 2,4,6-trimethylbenzene-1,3-diamine in bio-oil showed that 1,2,4-trimethoxybenzene was directly aminated (H18) by hydrazine obtained from the N-N coupling (P6) of amines from pyrolytic fragmentation of protein (P1).

The formation of 2,6-dimethoxyphenol and 2,6-dimethoxy-4-(2-propenyl)phenol indicated that the structure of lignin fractions in SB was dominated by the S-lignin and G-lignin, and therefore, the scission of β -ether bonds occurred via the concerted retro-ene fragmentation and Maccoll elimination mechanisms (L1, L5, L6, L12, L14, and L24). However, the additional formation of 2-ethylphenol was indicative of further derivation of the alkoxyphenols, i.e., 2-ethoxyphenol. The derivation route began with deprotonation of ethoxy substituent followed by a two-step radical rearrangement and protonation (L26) producing 2-(2-hydroxyethyl)phenol intermediate. Upon further dehydration and radical rearrangement (L27), this intermediate was converted into 2-ethylphenol. The 2-ethylphenol may be further derived into 4-*t*-butylstyrene. The E_2 elimination (L28) of hydroxyl group of 2-ethylphenol yielded ethylbenzene, which was converted into styrene upon hydrogenation (L29). Finally, the Friedel-Craft alkylation (L30) of styrene with *t*-butyl chloride produced 4-*t*-butylstyrene.

The formation of ketones (e.g., 2',6'-dimethoxyacetophenone and 3-methyl-1-(2,4,6-trihydroxyphenyl)-1-butanone) also demonstrated that the exothermic Friedel-Craft acylation occurred during MAFP of SB. The exothermic profile of this mechanism was verified by the reduced relative composition in the bio-oil derived from higher microwave power input. In addition, a cyclic C₅-ketone (i.e., 3-hydroxy-2-methylcyclopentane-1-one) was observed in the bio-oil, indicating the existence of the Piancatelli rearrangement (H17) of furfural (see the furfural formation mechanism explanation in subsection 3.3.1) during the process. The Piancatelli rearrangement involves a protonation-dehydration sequence that provides carbocations with two OH- groups allowing a 4 π electrocyclization ring closure [83]. Since the product of this reaction (e.g., 3-hydroxy-2-methylcyclopentane-1-one) was readily dehydrated (H8) into 2-methylcyclopent-2-ene-1-one and then hydrogenated (H9) into 2-methylcyclopenta-1,4-dien-1-ol, its relative content in the bio-oil decreased with microwave power input and processing time.

With relatively the same compositions of bio-oil as that of NS-derived bio-oil, the biogas composition was similarly composed of carbon dioxide, methane, propene, and hydrogen. However, the comparatively lower relative composition of hydrogen in SB-derived biogas was due to the reactivity of the resulting bio-oil constituents toward hydrogenation and dehydration reactions, e.g., 3-hydroxy-2-methylcyclopentane-1-one into 2-methylcyclopenta-1,4-dien-1-ol and 2-ethylphenol into styrene.

3.3.3. Orange seed (OS)

The increased formation of bio-oil from OS at higher microwave power input and longer processing time was greatly associated with the formation of aldehydes (e.g., 2-oxo-3-cyclopentene-1-acetaldehyde), ethers (e.g., 2-oxopropyl acetate), O-heterocyclics (e.g., 2-furanmethanol and 5-hydroxymethyl-2(5H)-furanone), N-heterocyclics (e.g., 1-(1H-pyrazol-4-yl)ethanone, 2-pyrrolidone, methyl-2-methyl-5-oxopyrrolidine-2-carboxylate, 3-methyl-4-propyl-2,5-dihydro-1H-pyrrole), and ketones (e.g., 3-methylcyclopent-2-en-1-one). However, the products of cleavage of β -ether bonds of lignin and subsequent derivation via the Friedel-Craft acylation (see detailed explanation in subsection 3.1.1) were still significant in the biocrude despite the lowered relative composition at higher reaction severity, e.g., 2-methoxyphenol, 2,6-dimethoxyphenol, 4-(4-hydroxy-3-methoxyphenyl)-2-butanone, and 1-(2,6-dihydroxy-4-methoxyphenyl)-1-butanone.

The aldehydes, ethers, and O-heterocyclics were obtained from cellulose derivatives via various endothermic mechanisms, e.g., glucose, 5-HMF, and furfural. The retro-aldol condensation (H26, H27) of glucose yielded glyceraldehyde. Upon a series of reduction (H29), dehydration

(H30), and oxidation (H31), glyceraldehyde was converted into 1-hydroxy-2-propanone that readily reacted with acetic acid (H32) forming 2-oxopropyl acetate [84]. The decarbonylation (H14) of 5-HMF yielded 2-furanmethanol. Moreover, 5-HMF may undergo the Baeyer-Villiger oxidation and 1,4-rearrangement producing 5-hydroxymethyl-2(5H)-furanone [85]. The endothermic Piancatelli rearrangement (H15) of furfural into 5-hydroxy-4,4-dimethyl-cyclopent-2-en-1-one [86], followed by oxidation of the hydroxyl group into carboxylic acid group yielded 2,2-dimethyl-5-oxocyclopent-3-ene-1-carboxylic acid (H20). Further demethylation (i.e., expelling methyl substituent as methane) and reduction of the carboxylic acid group produced 2-oxo-3-cyclopentene-1-acetaldehyde (H21).

The formation of N-heterocyclics in OS-derived bio-oil involved the α -dicarbonyls, dicarboxylic acid, amines, and hydrazines. The resulting amines from protein decomposition may couple to form hydrazines. The cyclocondensation between a suitable hydrazine acting as a bidentate nucleophile and a carbon unit including a 1,3-dicarbonyl compound (e.g., 3-oxobutanal) produced substituted pyrazoles, e.g., 1-(1H-pyrazol-4-yl)ethanone [87]. The protein-derived amines may directly react with other α -dicarbonyls via the Paal-Knorr reaction producing 3-methyl-4-propyl-1H-pyrrole [88,89]. This compound may be hydrogenated into 3-methyl-4-propyl-2,5-dihydro-1H-pyrrole. Moreover, pyrroles (e.g., 2-pyrrolidone) may be obtained from ring conversion of γ -butyrolactone via the reaction with primary amine/ammonia (L35) [90]. The γ -butyrolactone was produced from a series of reduction (L33) and dehydrogenative cyclization (L34) of 2-butyne-1,4-diol, which was the product of butynylation (L32) involving formaldehyde (i.e., a product of dehydroxymethylation of 5-HMF, H5) and acetylene, i.e., a product of C-C bond scission of styrene (L31) [91,92].

Meanwhile, the methyl 2-methyl-5-oxopyrrolidine-2-carboxylate was acquired through the cyclization (H13) of 2-methylenesuccinic acid with amines followed by esterification with methanol [93]. The 2-methylenesuccinic acid originated from the Baeyer-Villiger oxidation (H12) of levulinic acid, i.e., a product of 5-HMF rehydration (H12) [94]. The methanol came from demethoxylation of methoxy substituent of alkoxyphenols (L9).

3.3.4. Biochar formation

According to the literature for solid byproduct formation from thermochemical conversion of biomass [68], biochar was formed via repolymerization of bio-oil constituents. Since the detailed mechanisms of biochar formation have also been explained by Cao and coworkers [95] and Sudibyo and Tester [96], the mechanistic explanations on biochar formation focused on identifying the corresponding precursors and the thermodynamic behavior of potential precipitation reactions according to the literature. The precursors for biochar formation were identified based on the evolution of the relative composition in bio-oil.

The biochar formation during the MAFP of NS was caused by the repolymerization of aromatic aldehydes (e.g., 2-hydroxybenzaldehyde and 3,5-dimethoxy-4-hydroxycinnamaldehyde, P10) and aromatic ethers, e.g., 1,2,4-trimethoxybenzene and 1,2,4-trimethoxy-5-methylbenzene (H25). Sudibyo and Tester [96] have reported that aromatic aldehydes and ethers included the Knoevenagel, Pechmann, and Perkin aldol condensations, all of which are endothermic. As a result, higher microwave power input and longer processing time improved the yield of NS-derived biochar.

The biochar formation during the MAFP of SB and OS was underlain by the repolymerization of furans (e.g., furfural and 5-hydroxymethyl-2(5H)-furanone, H4 and H27), aromatic hydrocarbons (e.g., 4-*t*-butylstyrene, L20), amines (2,4,6-trimethylbenzene-1,3-diamine, H26), and ketone alcohols, e.g., 4-(4-hydroxy-3-methoxyphenyl)-2-butanone and 1-(2,6-dihydroxy-4-methoxyphenyl)-1-butanone (L37). These precursors were prone to the exothermic regioselective nucleophilic addition, Michael addition, Dieckmann cyclization, and oxidative and reductive coupling mechanisms involving the C-C and N-N bonds.

Given the exothermic nature of these reaction mechanisms, biochar formation was inhibited at higher reaction severity (i.e., higher microwave power input and extended processing time), giving a lower biochar yield.

4. Conclusions

This study investigated the mechanistic effects of microwave-assisted pyrolysis (MAFP) of three significant agricultural residues (i.e., pecan nutshell – NS, sugarcane bagasse – SB, and orange seed – OS) with diverse organic macromolecules compositions at different microwave power inputs (300–400 W) and processing times (3–5 min) on the yield and chemical composition of the products, i.e., bio-oil, biochar, and biogas. In general, higher microwave power input and prolonged processing times increased the bio-oil yield by promoting several endothermic reaction mechanisms with the prominent ones are as follows: (1) The heterolytic retro-ene fragmentation and Maccoll elimination, Friedel-Craft acylation, intramolecular cyclization, and methoxylation in the MAFP of NS. (2) The Friedel-Craft alkylation, Piancatelli rearrangement, and alkylation in the MAFP of SB. (3) The Maillard reaction, Paal-Knorr pyrrole synthesis, Baeyer-Villiger oxidation, and ring conversion of γ -butyrolactone. The biochar formation during the MAFP of NS was caused by the endothermic repolymerization of aromatic aldehydes (e.g., 2-hydroxybenzaldehyde and 3,5-dimethoxy-4-hydroxycinnamaldehyde) and aromatic ethers (e.g., 1,2,4-trimethoxybenzene and 1,2,4-trimethoxy-5-methylbenzene), thus, higher microwave power input and longer processing time improved the yield. The susceptibility of these bio-oil constituents to repolymerize into biochar provided lower biogas yield. In contrast, the biochar formation during the MAFP of SB and OS was caused by the exothermic repolymerization of furans (e.g., furfural and 5-hydroxymethyl-2(5H)-furanone), aromatic hydrocarbons (e.g., 4-*t*-butylstyrene), amines (2,4,6-trimethylbenzene-1,3-diamine), and ketone alcohols (e.g., 4-(4-hydroxy-3-methoxyphenyl)-2-butanone & 1-(2,6-dihydroxy-4-methoxyphenyl)-1-butanone), giving a lower biochar yield at higher microwave power input and longer processing time. The inhibited biochar formation resulted in abundant substituted-aromatics in bio-oil available for partial gasification via dealkylation, demethoxylation, decarbonylation, and dehydrogenation. Despite the different profiles of biogas yield, the main constituents of the resulting biogas were carbon dioxide, methane, propene, and hydrogen, with additional formation of acetylene and carbon monoxide for the OS-derived biogas due to the dehydroxymethylation of 5-hydroxymethyl) furfural and dealkylation of 2,6-dimethoxy-4-(2-propenyl)phenol, respectively. This study informed pivotal understandings of chemical phenomena occurring during MAFP of various biomass feedstocks. Future studies will focus on providing kinetic evidences to validate the mechanisms proposed using the heuristic graphical approach in this study.

CRedit authorship contribution statement

Ana Karen Silos-Llamas and **Hanifrahmawan Sudibyo** contributed equally: Methodology, Formal analysis, Investigation, Visualization, Writing – review & editing. **Virginia Hernández-Montoya**: Supervision, Funding acquisition, Supervision, Writing – review & editing. **Will Meredith**: Formal analysis, Methodology, Writing – review & editing. **Gabriela Durán-Jiménez**: Conceptualization, Supervision, Methodology, Formal analysis, Validation, Writing – review & editing.

Declaration of Competing Interest

The authors declare that they have no known competing financial interests or personal relationships that could have appeared to influence the work reported in this paper.

Data Availability

Data will be made available on request.

Acknowledgement

This research was supported by the Council of Science and Technology (CONACYT), Mexico under the grant 891197 and by TECNM (Project 7949.20-P).

Appendix A. Supporting information

Supplementary data associated with this article can be found in the online version at [doi:10.1016/j.jaap.2023.106217](https://doi.org/10.1016/j.jaap.2023.106217).

References

- [1] E.O. Ajala, J.O. Ighalo, M.A. Ajala, A.G. Adeniyi, A.M. Ayanshola, Sugarcane bagasse: a biomass sufficiently applied for improving global energy, environment and economic sustainability, *Bioresour. Bioprocess* 8 (2021), <https://doi.org/10.1186/s40643-021-00440-z>.
- [2] D.C. Martínez-Casillas, I. Mascorro-Gutiérrez, C.E. Arreola-Ramos, H.I. Villafán-Vidales, C.A. Arancibia-Bulnes, V.H. Ramos-Sánchez, A.K. Cuentas-Gallegos, A sustainable approach to produce activated carbons from pecan nutshell waste for environmentally friendly supercapacitors, *Carbon N. Y* 148 (2019) 403–412, <https://doi.org/10.1016/j.carbon.2019.04.017>.
- [3] M.S.N. do Santos, G.L. Zabet, M.A. Mazutti, G.A. Ugalde, K. Rezzadori, M.V. Tres, Optimization of subcritical water hydrolysis of pecan wastes biomasses in a semi-continuous mode, *Bioresour. Technol.* 306 (2020), 123129, <https://doi.org/10.1016/j.biortech.2020.123129>.
- [4] S. Suri, A. Singh, P.K. Nema, Current applications of citrus fruit processing waste: a scientific outlook, *Appl. Food Res.* 2 (2022), 100050, <https://doi.org/10.1016/j.afres.2022.100050>.
- [5] H. Sudibyo, M. Pecchi, J.W. Tester, Experimental-based mechanistic study and optimization of hydrothermal liquefaction of anaerobic digestates, *Sustain. Energy Fuels* 6 (2022) 2314–2329, <https://doi.org/10.1039/d2se00206j>.
- [6] S.O. Akinnowo, Eutrophication: Causes, consequences, physical, chemical and biological techniques for mitigation strategies, *Environ. Chall.* 12 (2023), <https://doi.org/10.1016/j.envc.2023.100733>.
- [7] J. Zhan, Y. Han, S. Xu, X. Wang, X. Guo, Succession and change of potential pathogens in the co-composting of rural sewage sludge and food waste, *Waste Manag.* 149 (2022) 248–258, <https://doi.org/10.1016/j.wasman.2022.06.028>.
- [8] A. Al-Rumaihi, M. Shahbaz, G. McKay, H. Mackey, T. Al-Ansari, A review of pyrolysis technologies and feedstock: a blending approach for plastic and biomass towards optimum biochar yield, *Renew. Sustain. Energy Rev.* 167 (2022), <https://doi.org/10.1016/j.rser.2022.112715>.
- [9] A. Dimitriadis, L.P. Chryssikou, G. Meletidis, G. Terzis, M. Auersvald, D. Kubička, S. Bezergianni, Bio-based refinery intermediate production via hydrodeoxygenation of fast pyrolysis bio-oil, *Renew. Energy* 168 (2021) 593–605, <https://doi.org/10.1016/j.renene.2020.12.047>.
- [10] A.A. Arpia, W.H. Chen, S.S. Lam, P. Rousset, M.D.G. de Luna, Sustainable biofuel and bioenergy production from biomass waste residues using microwave-assisted heating: a comprehensive review, *Chem. Eng. J.* 403 (2021), <https://doi.org/10.1016/j.cej.2020.126233>.
- [11] J. Fan, T.N. Kalnes, M. Alward, J. Klinger, A. Sadehvandi, D.R. Shonnard, Life cycle assessment of electricity generation using fast pyrolysis bio-oil, *Renew. Energy* 36 (2011) 632–641, <https://doi.org/10.1016/j.renene.2010.06.045>.
- [12] C. Wang, D. Luo, X. Zhang, R. Huang, Y. Cao, G. Liu, Y. Zhang, H. Wang, Biochar-based slow-release of fertilizers for sustainable agriculture: a mini review, *Environ. Sci. Ecotechnol.* 10 (2022), 100167, <https://doi.org/10.1016/j.ese.2022.100167>.
- [13] A. Kaithal, M. Hölscher, W. Leitner, Carbon monoxide and hydrogen (syngas) as a C1-building block for selective catalytic methylation, *Chem. Sci.* 12 (2021) 976–982, <https://doi.org/10.1039/d0sc05404f>.
- [14] K.N. Yogalakshmi, P.D. T. P. Sivashanmugam, S. Kavitha, Y.K. R. S. Varjani, S. Adishkumar, G. Kumar, R.B. J. Chemosphere Lignocellulosic biomass-based pyrolysis: A comprehensive review, 286 (2022).
- [15] J.J. Manyà, M. Azuara, J.A. Manso, Biochar production through slow pyrolysis of different biomass materials: seeking the best operating conditions, *Biomass-- Bioenergy* 117 (2018) 115–123, <https://doi.org/10.1016/j.biombioe.2018.07.019>.
- [16] R.E. Guedes, A.S. Luna, A.R. Torres, Operating parameters for bio-oil production in biomass pyrolysis: a review, *J. Anal. Appl. Pyrolysis* 129 (2018) 134–149, <https://doi.org/10.1016/j.jaap.2017.11.019>.
- [17] F.M. Baena-Moreno, D. Sebastia-Saez, L. Pastor-Pérez, T.R. Reina, Analysis of the potential for biogas upgrading to syngas via catalytic reforming in the United Kingdom, *Renew. Sustain. Energy Rev.* 144 (2021), <https://doi.org/10.1016/j.rser.2021.110939>.
- [18] T.A. Kurniawan, M.H.D. Othman, X. Liang, H.H. Goh, P. Gikas, K.K. Chong, K. W. Chew, Challenges and opportunities for biochar to promote circular economy and carbon neutrality, *J. Environ. Manag.* 332 (2023), <https://doi.org/10.1016/j.jenvman.2023.117429>.
- [19] Y.H. Chan, S.K. Loh, B.L.F. Chin, C.L. Yiin, B.S. How, K.W. Cheah, M.K. Wong, A.C. M. Loy, Y.L. Gwee, S.L.Y. Lo, S. Yusup, S.S. Lam, Fractionation and extraction of bio-oil for production of greener fuel and value-added chemicals: recent advances and future prospects, *Chem. Eng. J.* 397 (2020), <https://doi.org/10.1016/j.cej.2020.125406>.
- [20] J. Klinger, D.L. Carpenter, V.S. Thompson, N. Yancey, R.M. Emerson, K.R. Gaston, K. Smith, M. Thorson, H. Wang, D.M. Santosa, I. Kutnyakov, Pilot plant reliability metrics for grinding and fast pyrolysis of woody residues, *ACS Sustain. Chem. Eng.* 8 (2020) 2793–2805, <https://doi.org/10.1021/acssuschemeng.9b06718>.
- [21] W. Cai, A. Fivga, O. Kaario, R. Liu, Effects of torrefaction on the physicochemical characteristics of sawdust and rice husk and their pyrolysis behavior by thermogravimetric analysis and pyrolysis-gas chromatography/mass spectrometry, *Energy Fuels* 31 (2017) 1544–1554, <https://doi.org/10.1021/acs.energyfuels.6b01846>.
- [22] Q. Wang, H. Song, S. Pan, N. Dong, X. Wang, S. Sun, Initial pyrolysis mechanism and product formation of cellulose: an Experimental and Density functional theory (DFT) study, *Sci. Rep.* 10 (2020) 1–18, <https://doi.org/10.1038/s41598-020-60095-2>.
- [23] A. Osatiashtiani, J. Zhang, S.D. Stefanidis, X. Zhang, A.V. Bridgwater, The mechanism for catalytic fast pyrolysis of levoglucosan, furfural and furan over HZSM-5: an experimental and theoretical investigation, *Fuel* 328 (2022), 125279, <https://doi.org/10.1016/j.fuel.2022.125279>.
- [24] M. Carrier, R. Fournet, B. Sirjean, S. Amsbury, Y.B. Alfonso, P.Y. Pontalier, A. Bridgwater, Fast pyrolysis of hemicelluloses into short-chain acids: an investigation on concerted mechanisms, *Energy Fuels* 34 (2020) 14232–14248, <https://doi.org/10.1021/acs.energyfuels.0c02901>.
- [25] V.B.F. Custodis, P. Hemberger, Z. Ma, J.A. Van Bokhoven, Mechanism of fast pyrolysis of lignin: studying model compounds, *J. Phys. Chem. B* 118 (2014) 8524–8531, <https://doi.org/10.1021/jp5036579>.
- [26] Z. Luo, K. Lu, Y. Yang, S. Li, G. Li, Catalytic fast pyrolysis of lignin to produce aromatic hydrocarbons: optimal conditions and reaction mechanism, *RSC Adv.* 9 (2019) 31960–31968, <https://doi.org/10.1039/c9ra02538c>.
- [27] M. de Prá Andrade, D. Piazza, M. Poletto, Pecan nutshell: morphological, chemical and thermal characterization, *J. Mater. Res. Technol.* 13 (2021) 2229–2238, <https://doi.org/10.1016/j.jmrt.2021.05.106>.
- [28] M.A. Mahmud, F.R. Anannya, Sugarcane bagasse - A source of cellulosic fiber for diverse applications, *Heliyon.* 7 (2021) 1–14, <https://doi.org/10.1016/j.heliyon.2021.e07771>.
- [29] M.I. Akpator, P.I. Akubor, Chemical composition and selected functional properties of sweet orange (*Citrus sinensis*) seed flour, *Plant Foods Hum. Nutr.* 54 (1999) 353–362, <https://doi.org/10.1023/A:1008153228280>.
- [30] C.J. Donahue, E.A. Rais, Proximate analysis of coal, *J. Chem. Educ.* 86 (2009) 222–224, <https://doi.org/10.1021/ed086p222>.
- [31] G. Durán-Jiménez, L.A. Stevens, G.R. Hodgins, J. Uguna, J. Ryan, E.R. Binner, J. P. Robinson, Fast regeneration of activated carbons saturated with textile dyes: textural, thermal and dielectric characterization, *Chem. Eng. J.* 378 (2019), 121774, <https://doi.org/10.1016/j.cej.2019.05.135>.
- [32] G. Durán-Jiménez, E.T. Kostas, L.A. Stevens, W. Meredith, M. Erans, V. Hernández-Montoya, A. Buttress, C.N. Uguna, E. Binner, Green and simple approach for low-cost bioproducts preparation and CO₂ capture, *Chemosphere* 279 (2021), <https://doi.org/10.1016/j.chemosphere.2021.130512>.
- [33] G. Durán-Jiménez, J. Rodríguez, E.T. Kostas, L.A. Stevens, L. Lozada-Rodríguez, E. Binner, C. Dodds, Simultaneous conventional and microwave heating for the synthesis of adsorbents for CO₂ capture: comparative study to pristine technologies, *Chem. Eng. J.* 438 (2022), <https://doi.org/10.1016/j.cej.2022.135549>.
- [34] E.T. Kostas, G. Durán-Jiménez, B.J. Shepherd, W. Meredith, L.A. Stevens, O.S. A. Williams, G.J. Lye, J.P. Robinson, Microwave pyrolysis of olive pomace for bio-oil and bio-char production, *Chem. Eng. J.* 387 (2020), 123404, <https://doi.org/10.1016/j.cej.2019.123404>.
- [35] J.L. Andersen, C. Flamm, D. Merkle, P.F. Stadler, An intermediate level of abstraction for computational systems chemistry, *Philos. Trans. R. Soc. A Math. Phys. Eng. Sci.* 375 (2017), <https://doi.org/10.1098/rsta.2016.0354>.
- [36] F. Lu, C. Zhang, B. Lu, K. Yu, J. Liu, H. Kang, R. Liu, G. Lan, Cellobiose as a model compound for cellulose to study the interactions in cellulose/lithium chloride/N-methyl-2-pyrrolidone systems, *Cellulose* 24 (2017) 1621–1629, <https://doi.org/10.1007/s10570-017-1213-1>.
- [37] Y.P. Chen, Y.Q. Huang, J.J. Xie, X.L. Yin, C.Z. Wu, Hydrothermal reaction of phenylalanine as a model compound of algal protein, *Ranliuo Huaxue Xuebao/J. Fuel Chem. Technol.* 42 (2014) 61–67, [https://doi.org/10.1016/s1872-5813\(14\)60010-4](https://doi.org/10.1016/s1872-5813(14)60010-4).
- [38] B. Gomez-Monedero, J. Faria, F. Bimbela, M.P. Ruiz, Catalytic hydroprocessing of lignin β-O-4 ether bond model compound phenethyl phenyl ether over ruthenium catalysts, *Biomass-- Convers. Biorefinery* 7 (2017) 385–398, <https://doi.org/10.1007/s13399-017-0275-5>.
- [39] A.E. Coumans, E.J.M. Hensen, A model compound (methyl oleate, oleic acid, triolein) study of triglycerides hydrodeoxygenation over alumina-supported NiMo sulfide, *Appl. Catal. B Environ.* 201 (2017) 290–301, <https://doi.org/10.1016/j.apcatb.2016.08.036>.
- [40] J.L. Andersen, C. Flamm, D. Merkle, P.F. Stadler, Rule composition in graph transformation models of chemical reactions, *Match* 80 (2018) 661–704.
- [41] J.L. Andersen, C. Flamm, D. Merkle, P.F. Stadler, Chemical transformation motifs-modelling pathways as integer hyperflows, *IEEE/ACM Trans. Comput. Biol. Bioinforma.* 16 (2019) 510–523, <https://doi.org/10.1109/TCBB.2017.2781724>.
- [42] M.E. Beber, M.G. Gollub, D. Mozaffari, K.M. Shebek, A.I. Flamholz, R. Milo, E. Noor, EQuilibrator 3.0: a database solution for thermodynamic constant

- estimation, *Nucleic Acids Res* 50 (2022) D603–D609, <https://doi.org/10.1093/nar/gkab1106>.
- [43] D.M. Le, H.R. Sørensen, A.S. Meyer, Elemental analysis of various biomass solid fractions in biorefineries by X-ray fluorescence spectrometry, *Biomass.-. Bioenergy* 97 (2017) 70–76, <https://doi.org/10.1016/j.biombioe.2016.12.018>.
- [44] J.C.P. Vagheti, E.C. Lima, B. Royer, B.M. da Cunha, N.F. Cardoso, J.L. Brasil, S.L. P. Dias, Pecan nutshell as biosorbent to remove Cu(II), Mn(II) and Pb(II) from aqueous solutions, *J. Hazard. Mater.* 162 (2009) 270–280, <https://doi.org/10.1016/j.jhazmat.2008.05.039>.
- [45] G. Durán-Jiménez, V. Hernández-Montoya, M.A. Montes-Morán, M. Teutli-León, New oxygenated carbonaceous adsorbents prepared by combined radiant/microwave heating for the removal of Pb²⁺ in aqueous solution, *J. Anal. Appl. Pyrolysis* 113 (2015) 599–605, <https://doi.org/10.1016/j.jaap.2015.04.001>.
- [46] Z. Ma, Y. Yang, Y. Wu, J. Xu, H. Peng, X. Liu, W. Zhang, S. Wang, In-depth comparison of the physicochemical characteristics of bio-char derived from biomass pseudo components: hemicellulose, cellulose, and lignin, *J. Anal. Appl. Pyrolysis* 140 (2019) 195–204, <https://doi.org/10.1016/j.jaap.2019.03.015>.
- [47] D. Chen, K. Cen, X. Zhuang, Z. Gan, J. Zhou, Y. Zhang, H. Zhang, Insight into biomass pyrolysis mechanism based on cellulose, hemicellulose, and lignin: evolution of volatiles and kinetics, elucidation of reaction pathways, and characterization of gas, biochar and bio-oil, *Combust. Flame* 242 (2022), <https://doi.org/10.1016/j.combustflame.2022.112142>.
- [48] E. Leng, Y. Guo, J. Chen, S. Liu, J.E. Y. Xue, A comprehensive review on lignin pyrolysis: mechanism, modeling and the effects of inherent metals in biomass, *Fuel* 309 (2022), <https://doi.org/10.1016/j.fuel.2021.122102>.
- [49] W.H. Chen, J. Peng, X.T. Bi, A state-of-the-art review of biomass torrefaction, densification and applications, *Renew. Sustain. Energy Rev.* 44 (2015) 847–866, <https://doi.org/10.1016/j.rser.2014.12.039>.
- [50] R.K. Liew, W.L. Nam, M.Y. Chong, X.Y. Phang, M.H. Su, P.N.Y. Yek, N.L. Ma, C. K. Cheng, C.T. Chong, S.S. Lam, Oil palm waste: An abundant and promising feedstock for microwave pyrolysis conversion into good quality biochar with potential multi-applications, *Process Saf. Environ. Prot.* 115 (2018) 57–69, <https://doi.org/10.1016/j.psep.2017.10.005>.
- [51] A.K. Silos-Llamas, G. Durán-Jiménez, V. Hernández-Montoya, M.A. Montes-Morán, N.A. Rangel-Vázquez, Understanding the adsorption of heavy metals on oxygen-rich biochars by using molecular simulation, *J. Mol. Liq.* 298 (2020), 112069, <https://doi.org/10.1016/j.molliq.2019.112069>.
- [52] R. Liu, G. Liu, B. Yousaf, Z. Niu, Q. Abbas, Novel investigation of pyrolysis mechanisms and kinetics for functional groups in biomass matrix, *Renew. Sustain. Energy Rev.* 153 (2022), 111761, <https://doi.org/10.1016/j.rser.2021.111761>.
- [53] G. Durán-Jiménez, V. Hernández-Montoya, M.A. Montes-Morán, S.W. Kingman, T. Monti, E.R. Binner, Microwave pyrolysis of pecan nut shell and thermogravimetric, textural and spectroscopic characterization of carbonaceous products, *J. Anal. Appl. Pyrolysis* 135 (2018) 160–168, <https://doi.org/10.1016/j.jaap.2018.09.007>.
- [54] H.C. Ong, W.H. Chen, Y. Singh, Y.Y. Gan, C.Y. Chen, P.L. Show, A state-of-the-art review on thermochemical conversion of biomass for biofuel production: a TG-FTIR approach, *Energy Convers. Manag.* 209 (2020), 112634, <https://doi.org/10.1016/j.enconman.2020.112634>.
- [55] X. Peng, X. Ma, Y. Lin, Z. Guo, S. Hu, X. Ning, Y. Cao, Y. Zhang, Co-pyrolysis between microalgae and textile dyeing sludge by TG-FTIR: Kinetics and products, *Energy Convers. Manag.* 100 (2015) 391–402, <https://doi.org/10.1016/j.enconman.2015.05.025>.
- [56] A.B. Namazi, D.G. Allen, C.Q. Jia, Probing microwave heating of lignocellulosic biomasses, *J. Anal. Appl. Pyrolysis* 112 (2015) 121–128, <https://doi.org/10.1016/j.jaap.2015.02.009>.
- [57] G. Durán-Jiménez, L.A. Stevens, E.T. Kostas, V. Hernández-Montoya, J. P. Robinson, E.R. Binner, Rapid, simple and sustainable synthesis of ultra-microporous carbons with high performance for CO₂ uptake, via microwave heating, *Chem. Eng. J.* 388 (2020), 124309, <https://doi.org/10.1016/j.cej.2020.124309>.
- [58] J. Robinson, C. Dodds, A. Stavrinides, S. Kingman, J. Katrib, Z. Wu, J. Medrano, R. Overend, Microwave pyrolysis of biomass: Control of process parameters for high pyrolysis oil yields and enhanced oil quality, *Energy Fuels* 29 (2015) 1701–1709, <https://doi.org/10.1021/ef502403x>.
- [59] C. Zhao, E. Jiang, A. Chen, Volatile production from pyrolysis of cellulose, hemicellulose and lignin, *J. Energy Inst.* 90 (2017) 902–913, <https://doi.org/10.1016/j.joei.2016.08.004>.
- [60] A. Ahmed, M.S. Abu Bakar, R.S. Sukri, M. Hussain, A. Farooq, S. Moogi, Y.K. Park, Sawdust pyrolysis from the furniture industry in an auger pyrolysis reactor system for biochar and bio-oil production, *Energy Convers. Manag.* 226 (2020), 113502, <https://doi.org/10.1016/j.enconman.2020.113502>.
- [61] F. Campuzano, R.C. Brown, J.D. Martínez, Auger reactors for pyrolysis of biomass and wastes, *Renew. Sustain. Energy Rev.* 102 (2019) 372–409, <https://doi.org/10.1016/j.rser.2018.12.014>.
- [62] J. Chen, J. Zhang, W. Pan, G. An, Y. Deng, Y. Li, Y. Hu, Y. Xiao, T. Liu, S. Leng, J. Chen, J. Li, H. Peng, L. Leng, W. Zhou, A novel strategy to simultaneously enhance bio-oil yield and nutrient recovery in sequential hydrothermal liquefaction of high protein microalgae, *Energy Convers. Manag.* 255 (2022), 115330, <https://doi.org/10.1016/j.enconman.2022.115330>.
- [63] Y. Fan, U. Hornung, N. Dahmen, A. Kruse, Hydrothermal liquefaction of protein-containing biomass: study of model compounds for Maillard reactions, *Biomass.-. Convers. Biorefinery* 8 (2018) 909–923, <https://doi.org/10.1007/s13399-018-0340-8>.
- [64] J. Zhai, X. Han, Q. An, J. Liu, X. Jiang, Renewable nitrogen-containing products by Maillard reaction of sewage sludge and glucose. Part II. Fixed-bed co-pyrolysis of sewage sludge and glucose, *Fuel* 334 (2023), <https://doi.org/10.1016/j.fuel.2022.126797>.
- [65] R. Fahmi, A.V. Bridgwater, L.I. Darvell, J.M. Jones, N. Yates, S. Thain, I. S. Donnison, The effect of alkali metals on combustion and pyrolysis of Lolium and Festuca grasses, switchgrass and willow, *Fuel* 86 (2007) 1560–1569, <https://doi.org/10.1016/j.fuel.2006.11.030>.
- [66] H. Sudiby, K. Wang, J.W. Tester, Hydrothermal liquefaction of acid whey: effect of feedstock properties and process conditions on energy and nutrient recovery, *ACS Sustain. Chem. Eng.* 9 (2021) 11403–11415, <https://doi.org/10.1021/acssuschemeng.1c03358>.
- [67] H. Kawamoto, Lignin pyrolysis reactions, *J. Wood Sci.* 63 (2017) 117–132, <https://doi.org/10.1007/s10086-016-1606-z>.
- [68] S. Wang, G. Dai, H. Yang, Z. Luo, Lignocellulosic biomass pyrolysis mechanism: a state-of-the-art review, *Prog. Energy Combust. Sci.* 62 (2017) 33–86, <https://doi.org/10.1016/j.pecc.2017.05.004>.
- [69] X. Huang, C. Liu, J. Huang, H. Li, Theory studies on pyrolysis mechanism of phenethyl phenyl ether, *Comput. Theor. Chem.* 976 (2011) 51–59, <https://doi.org/10.1016/j.comptc.2011.08.001>.
- [70] M.T.T. Nguyen, N. Le, H.T. Nguyen, T.D.V. Luong, V.K.T. Nguyen, Y. Kawazoe, P. H. Tran, N.N. Pham-Tran, Mechanism of friedel-crafts acylation using metal triflate in deep eutectic solvents: an experimental and computational study, *ACS Omega* (2022), <https://doi.org/10.1021/acsomega.2c03944>.
- [71] F. Liu, L. Anand, M. Szostak, Diversification of indoles and pyrroles by molecular editing: new frontiers in heterocycle-to-heterocycle transmutation, *Chem. - A Eur. J.* 29 (2023), <https://doi.org/10.1002/chem.202300096>.
- [72] Z.J. Jain, P.S. Gide, R.S. Kankate, Biphenyls and their derivatives as synthetically and pharmacologically important aromatic structural moieties, *Arab. J. Chem.* 10 (2017) S2051–S2066, <https://doi.org/10.1016/j.arabjch.2013.07.035>.
- [73] M. Gandhi, D. Rajagopal, A. Senthil Kumar, Facile electrochemical demethylation of 2-methoxyphenol to surface-confined catechol on the mwcnt and its efficient electrocatalytic hydrazine oxidation and sensing applications, *ACS Omega* 5 (2020) 16208–16219, <https://doi.org/10.1021/acsomega.0c01846>.
- [74] N. Shi, Q. Liu, R. Ju, X. He, Y. Zhang, S. Tang, L. Ma, Condensation of α -carbonyl aldehydes leads to the formation of solid humins during the hydrothermal degradation of carbohydrates, *ACS Omega* 4 (2019) 7330–7343, <https://doi.org/10.1021/acsomega.9b00508>.
- [75] T.L. Lohr, Z. Li, T.J. Marks, Thermodynamic strategies for C–O bond formation and cleavage via tandem catalysis, *Acc. Chem. Res.* 49 (2016) 824–834, <https://doi.org/10.1021/acs.accounts.6b00069>.
- [76] K.L. Yearty, R.K. Maynard, C.N. Cortes, R.W. Morrison, A multioutcome experiment for the williamson ether synthesis, *J. Chem. Educ.* 97 (2020) 578–581, <https://doi.org/10.1021/acs.jchemed.9b00503>.
- [77] X. Wang, L. Sheng, X. Yang, Pyrolysis characteristics and pathways of protein, lipid and carbohydrate isolated from microalgae *Nannochloropsis* sp., *Bioresour. Technol.* 229 (2017) 119–125, <https://doi.org/10.1016/j.biortech.2017.01.018>.
- [78] A. Wnorowski, V.A. Yaylayan, Influence of pyrolytic and aqueous-phase reactions on the mechanism of formation of maillard products, *J. Agric. Food Chem.* 48 (2000) 3549–3554, <https://doi.org/10.1021/jf9913099>.
- [79] R. Li, X. Yin, S. Zhang, J. Yang, M. Zhao, Preparation and pyrolysis of two Amadori analogues as flavor precursors, *J. Anal. Appl. Pyrolysis* 160 (2021), 105357, <https://doi.org/10.1016/j.jaap.2021.105357>.
- [80] B. Grycová, I. Koutník, A. Prysacz, Pyrolysis process for the treatment of food waste, *Bioresour. Technol.* 218 (2016) 1203–1207, <https://doi.org/10.1016/j.biortech.2016.07.064>.
- [81] S. Lomate, B. Katryniok, F. Dumeignil, S. Paul, High yield lactic acid selective oxidation into acetic acid over a Mo–V–Nb mixed oxide catalyst, *Sustain. Chem. Process.* 3 (2015) 1–8, <https://doi.org/10.1186/s40508-015-0032-7>.
- [82] S. Yamaguchi, H. Kondo, K. Uesugi, K. Sakoda, K. Jitsukawa, T. Mitsudome, T. Mizugaki, H₂-free selective dehydroxymethylation of primary alcohols over palladium nanoparticle catalysts, *ChemCatChem* 13 (2021) 1135–1139, <https://doi.org/10.1002/cctc.202001866>.
- [83] G.T. Jaya, R. Insyani, J. Park, A.F. Barus, M.G. Sibi, V. Ranaware, D. Verma, J. Kim, One-pot conversion of lignocellulosic biomass to ketones and aromatics over a multifunctional Cu–Ru/ZSM-5 catalyst, *Appl. Catal. B Environ.* 312 (2022), 121368, <https://doi.org/10.1016/j.apcatb.2022.121368>.
- [84] S.M. Mahungu, S.L. Hansen, W.E. Artz, Volatile compounds in heated oleic acid-esterified propoxylated glycerol, *JAOCs J. Am. Oil Chem. Soc.* 75 (1998) 683–690, <https://doi.org/10.1007/s11746-998-0206-5>.
- [85] K. Mliki, M. Trabelsi, Efficient mild oxidation of 5-hydroxymethylfurfural to 5-hydroxymethyl-2(5H)-furanone, a versatile chemical intermediate, *Res. Chem. Intermed.* 42 (2016) 8253–8260, <https://doi.org/10.1007/s11164-016-2593-9>.
- [86] G. Arcile, J. Ouazzani, J.F. Betzer, Efficient Piancatelli rearrangement on a large scale using the Zippertex technology under subcritical water conditions, *React. Chem. Eng.* 7 (2022) 1640–1649, <https://doi.org/10.1039/d2re00098a>.
- [87] K. Karrouchi, S. Radi, Y. Ramli, J. Taoufik, Y.N. Mabkhot, F.A. Al-Aizari, M. Ansar, Synthesis and pharmacological activities of Pyrazole derivatives: A review, 2018, <https://doi.org/10.3390/molecules23010134>.
- [88] A.P. Pawar, J. Yadav, A.J. Dolas, Y.K. Nagare, E. Iype, K. Rangan, I. Kumar, Enantioselective direct synthesis of C3-hydroxyalkylated pyrrole via an amine-catalyzed aldol/paal-knorr reaction sequence, *Org. Lett.* 24 (2022) 7549–7554, <https://doi.org/10.1021/acs.orglett.2c02922>.
- [89] H. Sudiby, J.W. Tester, Sustainable resource recovery from dairy waste: a case study of hydrothermal Co-liquefaction of acid whey and anaerobic digestate mixture, *Energy Fuels* 37 (2023) 2897–2911, <https://doi.org/10.1021/acs.energyfuels.2c03860>.

- [90] Y.S. Yoon, H.K. Shin, B.S. Kwak, Ring conversion of γ -butyrolactone into N-methyl-2-pyrrolidone over modified zeolites, *Catal. Commun.* 3 (2002) 349–355, [https://doi.org/10.1016/S1566-7367\(02\)00138-3](https://doi.org/10.1016/S1566-7367(02)00138-3).
- [91] I.T. Trotsu, T. Zimmermann, F. Schüth, Catalytic reactions of acetylene: a feedstock for the chemical industry revisited, *Chem. Rev.* 114 (2014) 1761–1782, <https://doi.org/10.1021/cr400357r>.
- [92] Y. Ni, R.M. Kassab, M.V. Chevliakov, J. Montgomery, Total syntheses of isodomoic acids G and H: an exercise in tetrasubstituted alkene synthesis, *J. Am. Chem. Soc.* 131 (2009) 17714–17718, <https://doi.org/10.1021/ja907931u>.
- [93] V.L. Gein, T.A. Silina, A.A. Cherepanov, A.P. Shishkin, I.P. Bulatov, N. V. Dozmorova, R.R. Makhmudov, Synthesis and biological activity of 1-substituted 5-oxopyrrolidine-3-carboxylic acids, *Pharm. Chem. J.* 55 (2021) 23–25, <https://doi.org/10.1007/s11094-021-02366-4>.
- [94] M.J. Fink, M.D. Mihovilovic, Non-hazardous Baeyer-Villiger oxidation of levulinic acid derivatives: alternative renewable access to 3-hydroxypropionates, *Chem. Commun.* 51 (2015) 2874–2877, <https://doi.org/10.1039/c4cc08734h>.
- [95] X. Cao, J.J. Pignatello, Y. Li, C. Latta, M.A. Chappell, N. Chen, L.F. Miller, J. Mao, Characterization of wood chars produced at different temperatures using advanced solid-state ^{13}C NMR spectroscopic techniques, *Energy Fuels* 26 (2012) 5983–5991, <https://doi.org/10.1021/ef300947s>.
- [96] H. Sudibyo, J.W. Tester, Probing elemental speciation in hydrochar produced from hydrothermal liquefaction of anaerobic digestates using quantitative X-ray diffraction, *Sustain. Energy Fuels* 6 (2022) 5474–5490, <https://doi.org/10.1039/d2se01092e>.